Journal of Metals, Materials and Minerals, 35(4), e2402, 2025

Structural tuning of BiOI toward Bi_2O_3/AgI heterostructures via room-temperature ion exchange for improved photocatalytic activity

Varunya ATIMAYULERD[1], Sorawit THUEANBANGYANG[1], Kittiyaporn SINGSUMPHAN[1], Ganyaporn WONGWAEN[2], Cheewita SUWANCHAWALIT[2], and Montri AIEMPANAKIT[1,*]

[1] *Department of Physics, Faculty of Science, Silpakorn University, Thailand*
[2] *Department of Chemistry, Faculty of Science, Silpakorn University, Thailand*

***Corresponding author e-mail**: aiempanakit_m@su.ac.th

Received date:
11 May 2025
Revised date:
18 July 2025
Accepted date:
4 August 2025

Keywords:
BiOI-derived materials;
Ion exchange synthesis;
Heterojunction photocatalyst;
Visible-light photodegradation;
Indigo carmine

Abstract

In this work, a bismuth oxide/silver iodide (Bi_2O_3/AgI) heterojunction photocatalyst was successfully fabricated via a room-temperature ion exchange process using bismuth oxyiodide (BiOI) as a morphology-directing precursor. Building upon our previous work on solvent-modulated BiOI nanostructures, this study employs a chemical transformation route to develop interfacially connected heterostructures while preserving key morphological features. Structural, morphological, and optical characterizations, including X-ray diffraction, field-emission scanning electron microscopy, energy-dispersive X-ray spectroscopy, Fourier-transform infrared spectroscopy, and ultraviolet–visible diffuse reflectance spectroscopy, provided supporting evidence for the successful formation of Bi_2O_3/AgI heterojunctions with likely close interfacial contact. The optimized Bi_2O_3/AgI composite with a 50:50 mass ratio demonstrated the highest photocatalytic activity, enabling nearly complete degradation of indigo carmine within 30 min under visible-light irradiation, clearly outperforming both pristine Bi_2O_3 and AgI. The enhanced performance is attributed to efficient charge carrier separation and improved visible-light absorption enabled by favorable band alignment. These findings highlight the potential of BiOI-based ion-exchange strategies for designing efficient and scalable photocatalysts for environmental remediation.

1. Introduction

One pressing environmental issue is the widespread contamination of water bodies by organic dyes and industrial chemicals, particularly from textile, printing, and related industries [1]. These substances often exhibit high stability, rendering traditional remediation techniques ineffective. Consequently, visible-light-driven (VLD) photocatalysis has gained attention as an eco-friendly approach capable of degrading pollutants under solar or ambient illumination without the need for additional chemical agents [2-4].

Bismuth oxyiodide (BiOI) is widely recognized among VLD photocatalysts due to its suitable bandgap (~1.8 eV), layered matlockite-type crystal structure, and intrinsic electric field that collectively promote efficient separation of photogenerated charge carriers [5-7]. In many cases, BiOI adopts hierarchical flower-like architectures composed of nanosheet assemblies, which enhance visible-light absorption and provide abundant active sites for pollutant adsorption [8-10]. Nevertheless, the broader application of BiOI is hindered by rapid recombination of charge carriers and structural degradation under extended light exposure or in ionic aqueous conditions [11,12]. Various approaches have been developed to address these issues, including elemental doping [13], morphological tailoring, and heterojunction formation [14-16]. In particular, coupling BiOI with silver iodide (AgI) has attracted increasing attention owing to their synergistic band alignment and the strong visible-light response of AgI [17,18].

Numerous investigations have examined the fabrication of BiOI/AgI composite photocatalysts through co-precipitation or deposition methods, typically employing bismuth nitrate ($Bi(NO_3)_3$), silver nitrate ($AgNO_3$), and potassium iodide (KI) as precursor materials [19-21]. However, these techniques frequently result in disordered particle morphologies or compromise the hierarchical flower-like architecture of BiOI. For example, Cao *et al.* [19] reported that the introduction of silver ions (Ag^+) led to a significant disruption of the BiOI framework, yielding coarse particle agglomerates. Similarly, Wang *et al.* [20] and Reyna-Cavazos *et al.* [21] described BiOI-based systems in which the self-assembled nanosheet structures were no longer preserved. Although these studies involved the interaction between BiOI and Ag^+ or AgI, none explicitly aimed at synthesizing bismuth oxide (Bi_2O_3)/AgI heterostructures via a controlled phase transition mechanism.

Concurrently, heterostructures incorporating both Bi_2O_3 and AgI have also been studied for visible-light-driven photocatalysis. For instance, Xie *et al.* [22] developed a Z-scheme photocatalyst comprising graphene oxide (GO), AgI, and Bi_2O_3, while Yan *et al.* [23] introduced a complex multi-heterojunction configuration involving Ag–AgI/BiOI–Bi_2O_3. Despite their enhanced photocatalytic activities, these systems relied on additional components or uncontrolled synthesis pathways and did not specifically target the direct construction of a two-phase Bi_2O_3/AgI heterojunction derived from BiOI. Furthermore, efforts to retain the intrinsic flower-like morphology of BiOI during such transformations have been largely unsuccessful, despite this

architecture being well known for promoting light absorption and facilitating surface-mediated reactions [9,10].

Building upon our previous work that focused on solvent-mediated control of BiOI morphology, this study advances a chemically induced strategy using BiOI as a structural template to construct functional Bi_2O_3/AgI heterojunctions. The primary objective is to assess whether the hierarchical nanosheet-based architecture of BiOI can be partially retained and effectively integrated into the resulting heterostructures to enhance photocatalytic performance under visible-light irradiation. To achieve this, a mild-temperature ion-exchange method was employed, allowing simultaneous phase transformation and morphological preservation. Composites with varied BiOI-to-$AgNO_3$ mass ratios were synthesized and systematically evaluated. The findings highlight a morphology-guided, low-temperature synthesis approach for constructing Bi_2O_3/AgI heterostructures with improved photocatalytic activity, while bridging the gap between structural retention and practical heterojunction formation.

2. Experimental

2.1 Materials

Bismuth(III) nitrate pentahydrate ($Bi(NO_3)_3 \cdot 5H_2O$, 98%), $AgNO_3$ (≥99.9%), KI (≥99.5%), nitric acid (HNO_3, 70%), ethylene glycol (EG, ≥99.5%), sodium hydroxide (NaOH, >99%), and ethanol (99.9%) were purchased from commercial sources, including CARLO ERBA, Fisher Chemical, Ajax Finechem, RCI Labscan, Fisher Scientific, Pine Chemical, and CHEMIPAN. All reagents were of analytical grade. Deionized (DI) water was consistently used in all steps of the experimental procedure.

2.2 Synthesis of BiOI

The BiOI powder was prepared using a straightforward precipitation approach conducted at ambient temperature. Initially, 0.005 mol of $Bi(NO_3)_3 \cdot 5H_2O$ was added to 12.5 mL of diluted 2 M HNO_3 and stirred until fully dissolved. Subsequently, 87.5 mL of a 1:1 (v/v) mixture of DI water and EG was introduced under continuous agitation. In the next step, 0.001 mol of KI was dissolved in 100 mL of DI water and slowly added to the bismuth-containing solution. The pH of the mixture was adjusted to around 10 using 2 M NaOH, followed by stirring for 1 h. The resulting orange precipitate was separated by filtration, rinsed thoroughly with DI water and ethanol, and dried at 80°C for 24 h. This synthesis procedure was based on a prior study [24], which reported that a DI: EG ratio of 50:50 and pH ≈ 10 yielded BiOI with superior morphology for photocatalytic applications.

2.3 Synthesis of Bi_2O_3/AgI heterostructures

The fabrication of Bi_2O_3/AgI heterostructures is depicted in Figure 1. In this process, an aqueous solution of $AgNO_3$ at a concentration of 0.004 M was first prepared using deionized water, resulting in an inherent pH of approximately 4 without any external adjustment. Subsequently, 0.2 g of pre-synthesized BiOI powder was added to the solution and uniformly dispersed, and then introduced to the suspension to obtain BiOI: $AgNO_3$ mass ratios of 70:30, 50:50, and 30:70. To enhance mixing and interfacial interaction, the mixture was treated with ultrasonic waves for 30 min. This was followed by magnetic stirring at ambient temperature for 4 h to promote ion exchange. The resulting precipitate was separated by filtration, rinsed several times with DI water and ethanol, and dried at 105°C for 24 h. The resulting samples were labeled BA-70:30, BA-50:50, and BA-30:70 according to their respective mass ratios of BiOI and $AgNO_3$.

2.4 Synthesis of AgI

Briefly, pristine AgI was synthesized by directly mixing an aqueous solution of $AgNO_3$ (0.085 M) with an aqueous solution of KI (0.085 M) under constant stirring at room temperature. After stirring for 2 min, the precipitate was thoroughly washed several times with DI water and ethanol and then dried at 105°C for 24 h.

2.5 Characterizations

The crystalline phases of BiOI, AgI, and Bi_2O_3/AgI composites were identified by X-ray diffraction (XRD) using a Malvern Panalytical Aeris diffractometer with Cu Kα radiation with λ = 0.15406 nm, scanned over a 2θ range of 15° to 80°. The surface morphologies were examined using field emission scanning electron microscopy (FE-SEM), TESCAN MIRA3, while the elemental composition and distribution were analyzed via energy-dispersive X-ray spectroscopy (EDS) operated at 20 kV. Fourier-transform infrared spectroscopy (FT-IR) spectra were monitored in transmittance mode (400 cm^{-1} to 4000 cm^{-1}) using a Perkin Elmer Spectrum BX to identify functional groups. The optical absorption properties were evaluated using UV–visible diffuse reflectance spectroscopy (DRS) with a Shimadzu UV2401 UV–Vis spectrophotometer.

2.6 Photocatalytic experiments

The photocatalytic degradation activity of the samples was investigated by tracking the visible-light-induced degradation of indigo carmine (IC). In a typical test, 0.05 g of BiOI, AgI, or Bi_2O_3/AgI catalyst was dispersed in 50 mL of a 5×10^{-5} M IC aqueous solution. Before irradiation, the suspension was kept under dark conditions, stirring for 30 min to allow adsorption–desorption equilibrium between the dye and the catalyst surface. Subsequently, two 18 W daylight lamps (Philips TL-D 18W/865) with no filter were placed above the reaction vessel to initiate visible-light illumination. The solution pH was initially ~5 and remained unadjusted throughout the experiment [25].

At specified time intervals (5 min), 3 mL aliquots of the suspension were withdrawn, centrifuged to remove particulates, and analyzed by Thermo-Orion AquaMate 8000 UV–Vis spectrophotometry at a wavelength of 611 nm to determine the residual IC concentration [26,27]. The degradation efficiency was calculated using the following Equation (1)

$$\% \text{ Degradation} = \left(\frac{C_0 - C_t}{C_0}\right) \times 100 \quad (1)$$

where C_0 and C_t denote the concentrations of IC at the initial time and at time t, respectively.

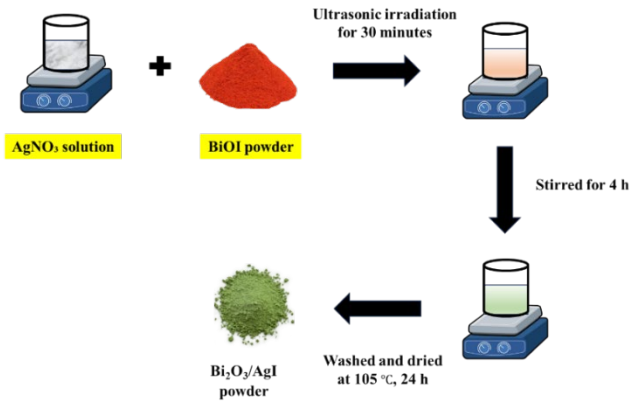

Figure 1. Schematic diagram of the fabrication process of the Bi_2O_3/AgI heterostructures.

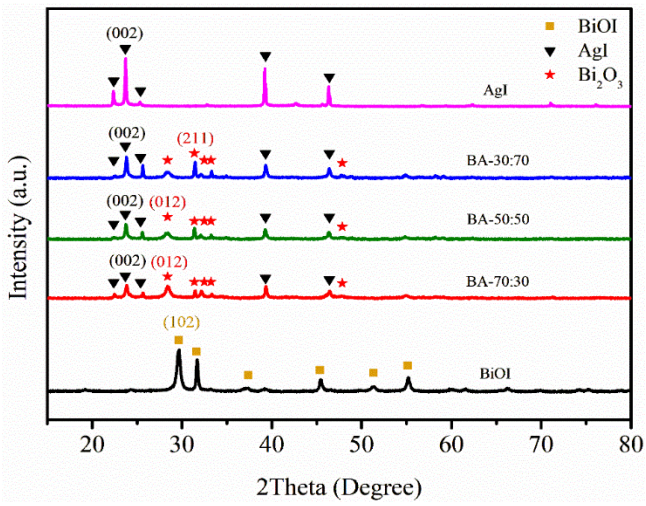

Figure 2. XRD patterns of BiOI, AgI, and Bi_2O_3/AgI composites prepared with different BiOI: $AgNO_3$ mass ratios.

2.7 Radicals quenching experiments

To elucidate the reactive species responsible for the photocatalytic degradation mechanism of Bi_2O_3/AgI, radical scavenging experiments were performed using the same experimental setup described above. Specific quenchers were added individually to the reaction system to selectively inhibit different reactive species. Benzoquinone (BQ, 0.01 M) was employed as a scavenger for superoxide radicals ($^{\bullet}O_2^-$), 0.01 M ethylenediaminetetraacetic acid (EDTA, 0.01 M) was used to capture photogenerated holes (h^+), and tert-butyl alcohol (*t*-butanol) was introduced to quench hydroxyl radicals ($^{\bullet}OH$) [28]. The reduction in photocatalytic degradation efficiency upon the addition of each scavenger was used to infer the relative contribution of the corresponding reactive species in the overall degradation process.

3. Results and discussion

3.1 Crystal structure

The crystalline phases of BiOI, AgI, and Bi_2O_3/AgI composites were characterized by XRD, as shown in Figure 2. The diffraction peaks observed at $2\theta = 22.39°$, 23.68°, 25.37°, 39.30°, and 45.40° correspond to the (100), (002), (101), (110), and (200) planes of hexagonal AgI (JCPDS No. 09-0374) [29,30]. For BiOI, six prominent peaks at 29.64°, 31.66°, 37.39°, 45.37°, 51.34°, and 55.12° were identified, which match the (102), (110), (112), (200), (114), and (212) planes of tetragonal BiOI (JCPDS No. 10-0445) [31]. In the BA-70:30, BA-50:50, and BA-30:70 composite samples, the diffraction patterns exhibited peaks corresponding to both AgI and monoclinic β-Bi_2O_3 (JCPDS No. 41-1449) [32]. Notably, the diffraction peaks of BiOI were absent in these samples, suggesting that BiOI was fully consumed or converted during the ion exchange process, with no residual peaks detected. The ion exchange between Ag^+ and BiOI is proposed to induce the phase transformation to Bi_2O_3, while AgI nucleates in situ on the surface [31]. Although the peak at $2\theta = 28.39°$ is typically the main reflection of Bi_2O_3, the relative increase of the 31.38° peak does not indicate a phase change but rather reflects alterations in crystallographic orientation or crystallinity. The presence of multiple diffraction peaks consistent with JCPDS patterns confirms that the material remains in the Bi_2O_3 phase. Additionally, as the $AgNO_3$ ratio increased, the intensity of the AgI (002) peak increased, indicating a higher AgI content in the composite. No impurity peaks were detected in any of the samples, confirming the high purity of the synthesized materials. Although quantitative phase analysis via Rietveld refinement was not performed, the elemental composition data from EDS analysis revealed a steady increase in Ag content and a decreasing trend in O content with higher $AgNO_3$ ratios. These changes are consistent with the transformation of BiOI into AgI and Bi_2O_3, as observed in the XRD patterns. In our experiments, the hierarchical BiOI architectures were utilized as an iodine source to react with Ag^+ in solution through an ion-exchange mechanism, leading to the formation of the Bi_2O_3/AgI photocatalyst, as illustrated in Equation (2).

$$2BiOI\ (s) + 2Ag^+\ (aq) + H_2O \rightarrow 2AgI\ (s) + Bi_2O_3(s) + 2H^+ \quad (2)$$

Table 1. XRD data and crystallite size of BiOI, AgI, and Bi_2O_3/AgI samples calculated using the Scherrer equation.

Sample	Crystalline size [nm]		
	BiOI Peak (29.64°)	**Bi_2O_3 Peak (28.39°)**	**AgI Peak (23.68°)**
BiOI	17.66	-	-
BA-70:30	-	15.88	44.47
BA-50:50	-	12.66	36.39
BA-30:70	-	13.28	38.12
AgI	-	-	61.72

Note: The crystallite sizes were estimated using the (002) peak of AgI at $2\theta = 23.68°$ and the (012) peak of Bi_2O_3 near 28.39°, where applicable. The reduction in crystallite size in the composite samples may be attributed to interface effects and co-growth of Bi_2O_3 and AgI during ion exchange.

The crystallite size (D) of selected peaks was estimated using the Scherrer equation (Equation (3))

$$D = \frac{k\lambda}{\beta \cos\theta} \quad (3)$$

where D is the crystallite size, k = 0.89 is the shape factor, λ = 0.154 nm is the X-ray wavelength, β is the full width at half maximum (FWHM) of the reflection, and θ is the Bragg angle. The crystallite size of the Bi_2O_3 was estimated based on the main diffraction peak (28.39°) to be around 12 nm to 16 nm. The overall crystallite size of the BA-70:30, BA-50:50, and BA-30:70 is smaller than that of pristine AgI of 61.72 nm at the (002) plane, which might be due to the hybriding of AgI with Bi_2O_3 as summarized in Table 1.

3.2 Morphology and elemental distribution

The surface morphology of BiOI, Bi_2O_3/AgI composites, and AgI was examined using FE-SEM, as shown in Figure 3. The pristine BiOI sample exhibited a well-defined, flower-like morphology composed of self-assembled nanosheets (Figure 3(a)). This hierarchical structure benefits photocatalytic applications due to its large surface area and effective light scattering, which enhance pollutant adsorption and reaction efficiency [9,10]. Interestingly, this characteristic nanosheet assembly was partially retained in the BA-70:30 and BA-50:50 composites (Figure 3(b–c)), even after Ag^+-induced ion exchange. Although the nanosheets appeared slightly aggregated and less ordered with increasing $AgNO_3$ content, the overall morphology of BA-50:50 still retained the flower-like structure more clearly than BA-30:70. This morphological retention is a key distinction of the present work compared to previous reports where co-precipitation or strong etching methods often destroyed the BiOI architecture [19, 20]. For BA-30:70 (Figure 3(d)), the nanosheet features were largely lost and replaced by more agglomerated particles, indicating that excessive $AgNO_3$ may disturb the structural integrity of BiOI. The AgI sample (Figure 3(e)) exhibited spherical, randomly distributed particles with an average size of approximately 1 μm, consistent with previous studies [33]. To verify elemental distribution, EDS analysis was performed on the BA-50:50 sample. Figure 4(a) shows the corresponding FE-SEM image, while Figure 4(b–e) display the elemental mapping of Bi, O, I, and Ag, respectively. The mappings demonstrate a homogeneous distribution of all constituent elements across the composite surface. The atomic percentages of Bi, O, I, and Ag obtained from EDS spectra are summarized in Table 2. The data confirm the coexistence of Bi_2O_3 and AgI within the samples and reflect the trend of increasing Ag content as the $AgNO_3$ loading increases. No impurity elements were detected, which supports the high phase purity observed in the XRD results.

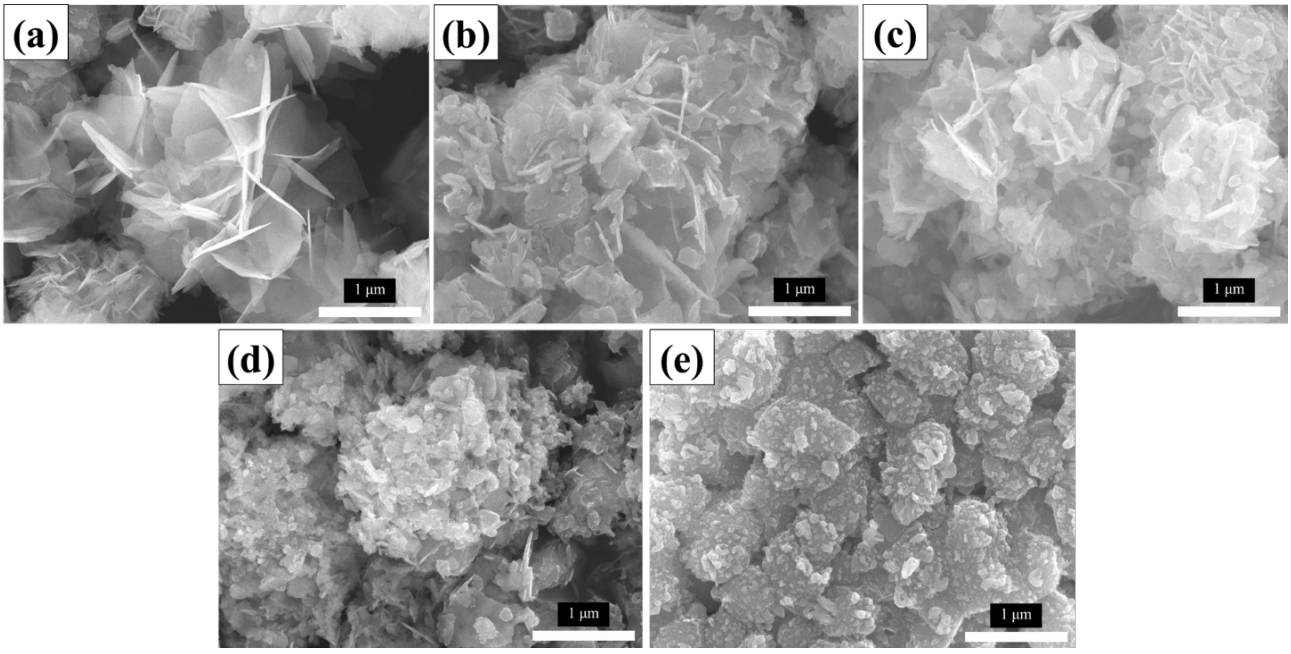

Figure 3. FE-SEM images of (a) BiOI, (b) BA-70:30, (c) BA-50:50, (d) BA-30:70, and (e) AgI.

Table 2. Atomic percentages of Bi, O, I, and Ag in each sample obtained from EDS analysis.

Sample	Atomic percentages			
	Bi	**O**	**I**	**Ag**
BiOI	30.66	35.75	33.59	-
BA-70:30	21.50	42.21	21.20	15.10
BA-50:50	20.80	39.50	21.80	18.17
BA-30:70	20.64	23.50	30.74	25.12
AgI	-	-	48.42	51.58

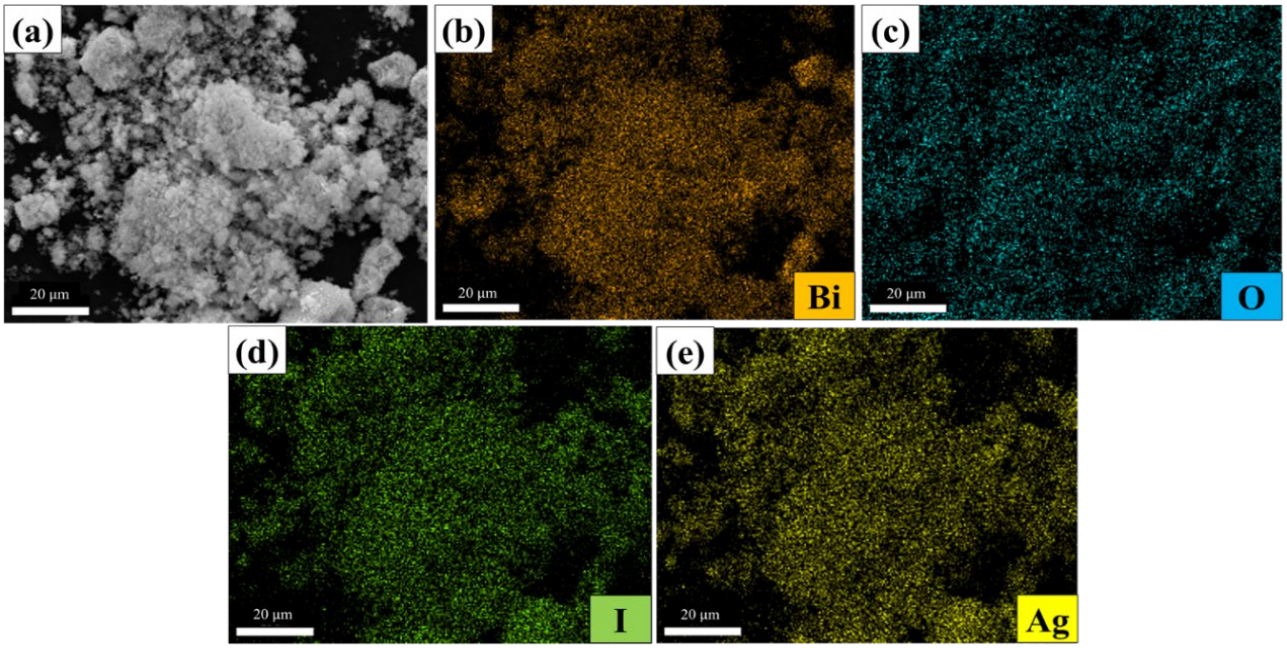

Figure 4. (a) Elemental mapping of BA-50:50 showing, (b) Bi, (c) O, (d) I, and (e) Ag.

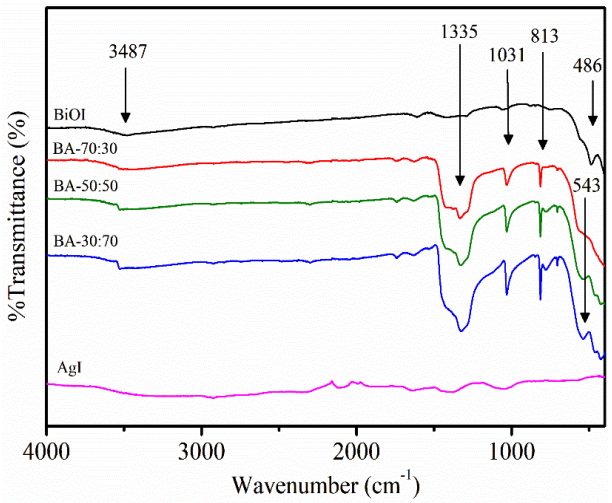

Figure 5. FT-IR spectra of BiOI, AgI, and Bi_2O_3/AgI composites synthesized at different BiOI: $AgNO_3$ mass ratios, illustrating the evolution of chemical bonding features associated with Bi–O and Ag–I vibrations.

3.3 FT-IR analysis

The chemical bonding characteristics of BiOI, AgI, and Bi_2O_3/AgI composites were examined using FT-IR, as presented in Figure 5. In the pristine BiOI spectrum, a prominent absorption band around 486 cm^{-1} is attributed to the Bi–O stretching vibration. A distinct band at 543 cm^{-1}, observed in AgI, corresponds to the Ag–I vibrational mode [23]. For the Bi_2O_3/AgI composites, additional peaks emerged at 813 cm^{-1} and 1335 cm^{-1}, characteristic of Bi–O stretching vibrations in the monoclinic Bi_2O_3 phase. Furthermore, a peak at 1031 cm^{-1} may be associated with asymmetric Bi–O vibrations, potentially arising from local lattice disorder or surrounding structural interactions [34]. The band near 3487 cm^{-1} is attributed to surface-bound O–H groups [35]. These surface hydroxyls may also contribute to photocatalytic activity by participating in radical generation during irradiation. The gradual appearance and intensification of Bi_2O_3 and AgI-related peaks, along with the reduction of BiOI characteristic signals, support the occurrence of phase transformation through the Ag^+-induced ion exchange process. This confirms the successful formation of Bi_2O_3/AgI heterostructures and provides spectroscopic evidence of the structural conversion.

3.4 Optical properties

The optical absorption behavior of BiOI, AgI, and Bi_2O_3/AgI composites was analyzed using DRS, as shown in Figure 6(a). All Bi_2O_3/AgI composites (BA-70:30, BA-50:50, and BA-30:70) exhibited strong absorption in the visible region with absorption edges located near 435 nm, indicating their suitability for visible-light-driven photocatalysis.

The optical band gap energy (E_g) was employed using the Tauc relation (Equation (4)).

$$(\alpha h\upsilon)^{1/n} = A(h\upsilon - E_g) \quad (4)$$

where α is the absorption coefficient, h is Planck's constant, υ is the photon frequency, and A is a constant. The E_g of BA-70:30, BA-50:50, and BA-30:70 was found to be approximately 2.87 eV, with minor variations among compositions, as shown in Figure 6(b). For indirect band gap semiconductors, such as BiOI, n = 2, whereas for direct band gap semiconductors, like AgI, n = 1/2 [23]. The Tauc plot of $(\alpha h\upsilon)^{1/2}$ and $(\alpha h\upsilon)^2$ versus hυ was obtained, as shown in Figure 6(c). The E_g of BiOI and AgI were 1.92 eV and 2.84 eV, respectively. These values align well with previously reported data [36,37], confirming the band gap of BiOI and AgI.

To further analyze the charge transfer behavior, the valence band edge (E_{VB}) and conduction band edge (E_{CB}) positions were calculated using the following empirical (Equations (5)-(6)).

$$E_{VB} = \chi - E_e + 0.5E_g \quad (5)$$

$$E_{CB} = E_{VB} - E_g \quad (6)$$

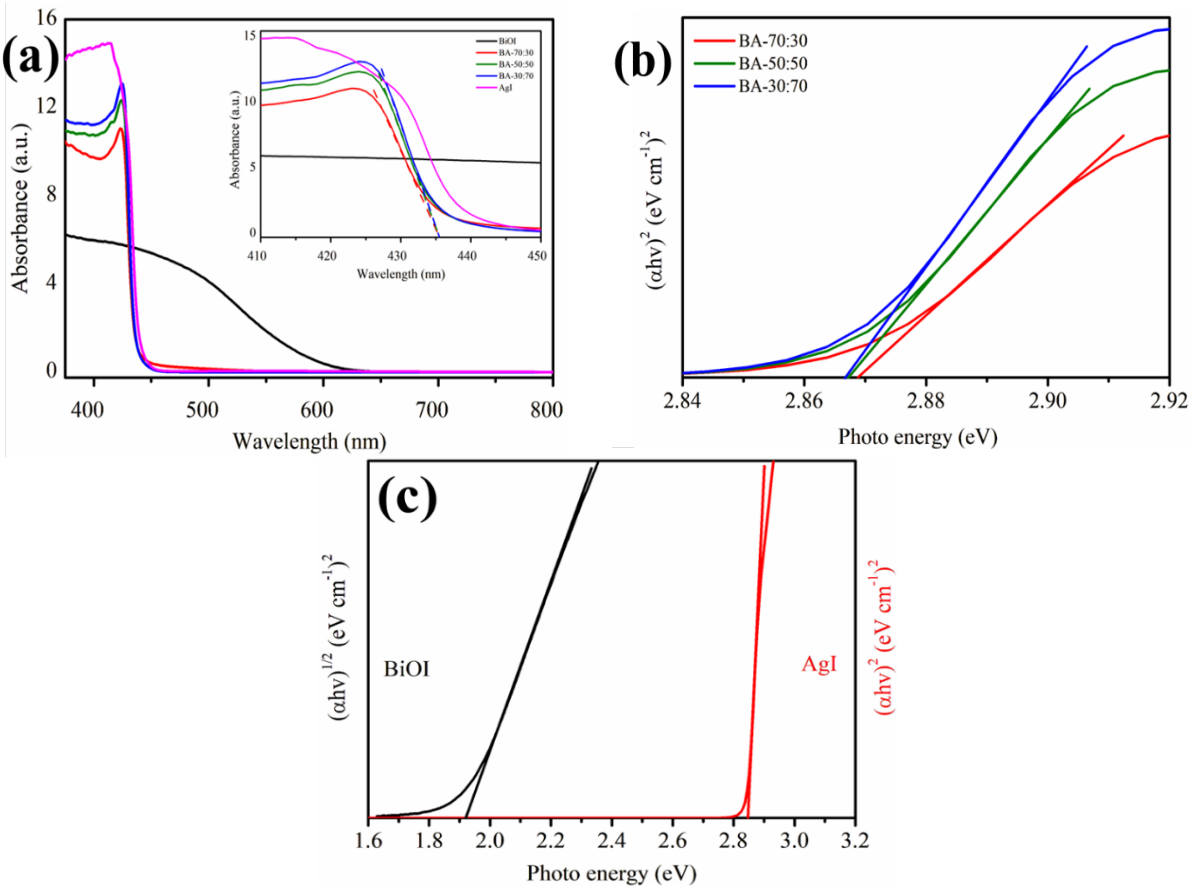

Figure 6. (a) UV–Vis DRS spectra of BiOI, AgI, and Bi_2O_3/AgI composites, (b) Tauc plots for BA-70:30, BA-50:50, and BA-30:70, and (c) BiOI (indirect) and AgI (direct) band gap calculations.

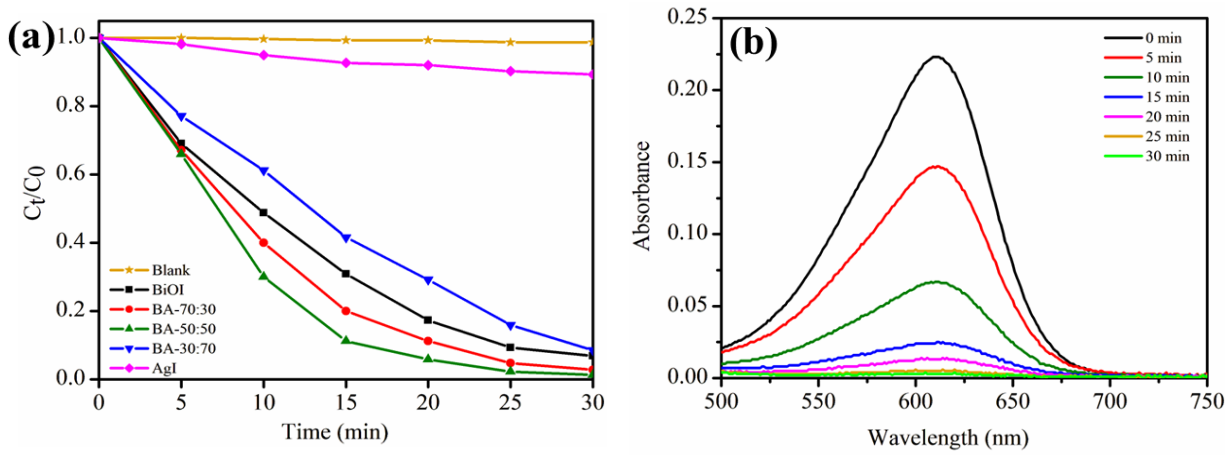

Figure 7. (a) Comparison of IC degradation with and without catalysts under visible light (blank = IC solution only) and (b) UV–Vis absorption spectra of IC degradation by BA-50:50 over time.

where χ is the absolute electronegativity of the semiconductor, and E_e is the energy of free electrons on the hydrogen scale (4.5 eV). The values of χ for Bi_2O_3 and AgI are 6.24 eV and 5.48 eV, respectively [22]. Using these equations and an assumed E_g of 2.85 eV for Bi_2O_3 [40,41], the E_{VB} and E_{CB} positions were estimated to be 3.17 eV and 0.32 eV for Bi_2O_3, and 2.40 eV and –0.44 eV for AgI, respectively. This band alignment facilitates directional migration of photogenerated charge carriers across the Bi_2O_3/AgI interface, which is favorable for enhanced photocatalytic activity under visible light.

3.5 Photocatalytic performance and reactive species identification

The photocatalytic activity of the synthesized samples was evaluated by degrading IC under visible light irradiation, as shown in Figure 7(a). The photolysis of IC was not observed in the blank experiment conducted at pH 5, indicating that IC is highly stable under visible light and that both photolysis and dye-sensitized degradation processes are negligible. Pure AgI showed poor photocatalytic efficiency, with only about 10%

degradation of IC after 30 min. In contrast, BiOI achieved around 93% degradation under the same conditions. When Bi_2O_3/AgI composites were used, a significant improvement was observed, especially for the BA-50:50 sample, which reached 99% degradation within 30 min. The BA-70:30 sample also showed high activity, while BA-30:70 had slightly lower performance (91%), suggesting that an excessive AgI content might hinder photocatalytic efficiency. These differences could be attributed to changes in charge separation dynamics and surface reactivity [38,39]. During the degradation process, the absorbance of IC at 611 nm gradually decreased with time, indicating a steady reduction in concentration. No new absorption peaks were observed, which suggests that no detectable intermediate products were formed and that IC was completely broken down, as shown in Figure 7(b).

The degradation reaction followed pseudo-first-order kinetics, as described by the following Equation (7).

$$\ln\left(\frac{C_t}{C_0}\right) = -kt \quad (7)$$

where the parameter k represents the rate constant for pseudo-first-order kinetics governing the degradation of IC. The simulated kinetic curves and corresponding rate constant k (min^{-1}) are shown in Figure 8. The k values for BiOI, BA-70:30, BA-50:50, BA-30:70 and AgI were 0.0934, 0.1234, 0.1523, 0.0470, and 0.0038 min^{-1}, respectively. The k value of BA-50:50 was approximately 1.6 time greater than that of BiOI and about 40 time greater than that of AgI under the same conditions. These findings underscore the optimized performance of BA-50:50, likely due to balanced charge transfer and interfacial contact within the heterojunction.

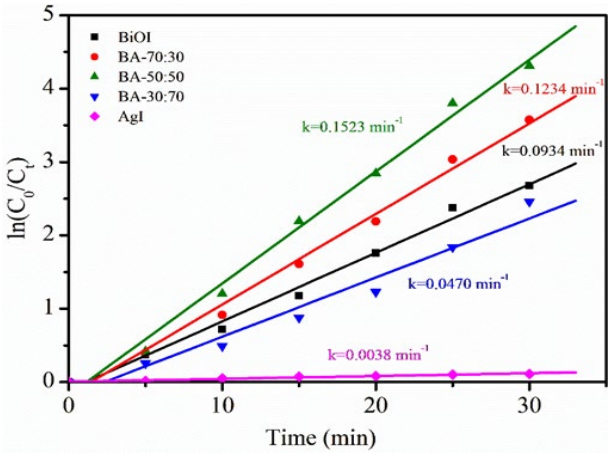

Figure 8. Kinetic plots and corresponding rate constants of IC degradation.

Table 3 presents a comparative analysis of Bi_2O_3/AgI photocatalysts with varying structural morphologies, dye, and experimental conditions. Notably, the flower-like structure synthesized in this study demonstrated superior activity under comparable conditions, with performance that is competitive with or exceeds that of previously reported Bi_2O_3/AgI systems.

The stability of the BA-50:50 sample was evaluated by performing three consecutive degradation cycles under visible light, as shown in Figure 9. A gradual decrease in efficiency was observed across 3 cycles. Nevertheless, the degradation efficiency remained above 50% in all cycles. This decline may be due to surface fouling from residual degradation products [40,41].

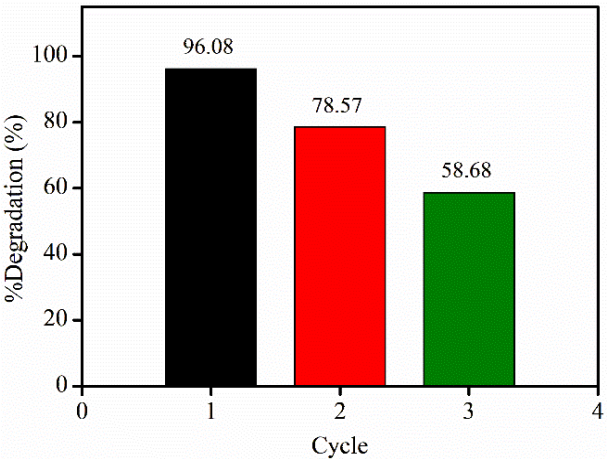

Figure 9. Recyclability test results for BA-50:50 under visible light.

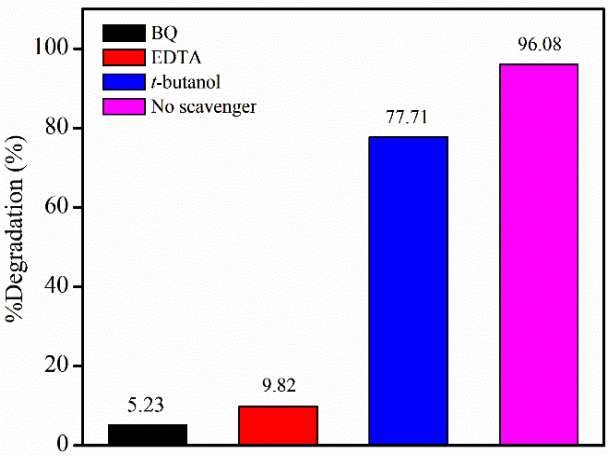

Figure 10. Radical scavenging results for IC degradation using BA-50:50.

Table 3. Summary of photocatalytic efficiencies of structurally diverse catalysts across different dye systems.

Samples	Structure	Concentration of dye	% Degradation and time	Ref.
Bi_2O_3/AgI	AgI NPs Bi_2O_3 flat-sphere	Rhodamine B (1×10^{-5} M)	97% and 60 min	[20]
Bi_2O_3/AgI	AgI spherical Bi_2O_3 flower-like	Methyl orange (20 mg·L^{-1})	95% and 60 min	[22]
Ag-AgI/BiOI-Bi_2O_3	BiOI nanosheets AgI NPs Bi_2O_3 flake-like	Methyl orange (20 mg·L^{-1})	95% and 60 min	[23]
Bi_2O_3/AgI	AgI spherical Bi_2O_3 flower-like	IC (5×10^{-5} M)	99% and 30 min	This work

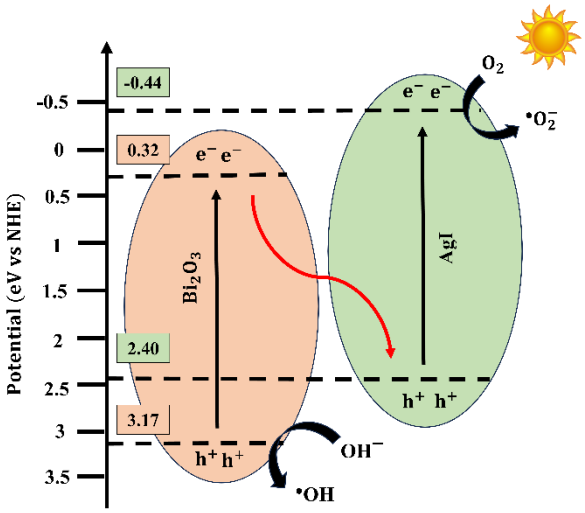

Figure 11. Schematic illustration of the proposed Z-scheme photocatalytic degradation mechanism of IC over Bi_2O_3/AgI heterostructures under visible-light irradiation.

To investigate the active species involved in the photocatalytic reaction, radical quenching experiments were conducted using BQ for $^{\bullet}O_2^-$, EDTA for h^+, and *t*-butanol for $^{\bullet}OH$. As shown in Figure 10, adding BQ and EDTA led to a significant reduction in degradation efficiency, indicating that $^{\bullet}O_2^-$ and h^+ were the main reactive species. The presence of *t*-butanol had a smaller effect, suggesting that $^{\bullet}OH$ contributed only marginally to the overall photocatalytic activity [23].

3.6 Proposed photocatalytic mechanism

The proposed mechanism for IC degradation over the Bi_2O_3/AgI composite (BA-50:50) is presented in Figure 11. Upon exposure to visible light, both Bi_2O_3 and AgI are photoexcited to generate electron–hole (e^-/h^+) pairs. In a Z-scheme heterojunction, only the photogenerated e^- in the conduction band (CB) of Bi_2O_3 transfers to the photogenerated h^+ in the valence band (VB) of AgI, facilitating effective charge separation while preserving the strong redox potentials of both semiconductors. The efficient charge transition resulted in the accumulation of the e^- on the conduction band of AgI and h^+ on the valence band of Bi_2O_3, which achieved an efficient separation of the electron-hole pairs and a decrease of the inner self-recombination of the semiconductors. Furthermore, the electrons in the CB of AgI would reduce the O_2 to $^{\bullet}O_2^-$ radical due to the more negative potential and part of the h^+ in the VB of Bi_2O_3 would generate the $^{\bullet}OH$ radicals [23,42]. This mechanistic pathway is consistent with the radical scavenging results, which identified $^{\bullet}O_2^-$ and h^+ as the dominant reactive species, with $^{\bullet}OH$ contributing a secondary role. Photocatalytic degradation of IC involves cleavage of the conjugated –C=C– and –C–N– bonds within its chromophore structure, leading to the loss of color and molecular breakdown [43,44]. In this study, the oxidative species generated by Bi_2O_3/AgI, particularly $^{\bullet}O_2^-$ and h^+, are believed to selectively attack these bonds, thereby initiating the degradation process of the dye molecule. The key photocatalytic steps are summarized below (Equations (8)-(14)).

$$Bi_2O_3 \xrightarrow{h\upsilon} Bi_2O_3\,(e^-_{CB} + h^+_{VB}) \quad (8)$$

$$AgI \xrightarrow{h\upsilon} AgI\,(e^-_{CB} + h^+_{VB}) \quad (9)$$

$$AgI\,(e^-_{CB}) + O_2 \rightarrow {}^{\bullet}O_2^- \quad (10)$$

$$H_2O + h^+ \rightarrow {}^{\bullet}OH + OH^- \quad (11)$$

$$Bi_2O_3\,(h^+) + IC \rightarrow \text{degradation products} \quad (12)$$

$$^{\bullet}O_2^- + IC \rightarrow \text{degradation products} \quad (13)$$

$$^{\bullet}OH + IC \rightarrow \text{degradation products} \quad (14)$$

This proposed Z-scheme charge transfer mechanism effectively accounts for the enhanced photocatalytic activity observed in the BA-50:50 composite. Although the estimated E_g values of BA-70:30, BA-50:50, and BA-30:70 are relatively similar, the improved performance of BA-50:50 may be attributed to its reduced crystallite size, which increases grain boundary density and promotes interfacial charge migration. Furthermore, the Z-scheme configuration enables directional charge transfer while retaining the strong redox potentials of both Bi_2O_3 and AgI, thereby maximizing the separation efficiency of photogenerated charge carriers and resulting in significantly enhanced visible-light-driven photocatalytic activity [22,23].

4. Conclusion

In summary, Bi_2O_3/AgI heterojunction photocatalysts were successfully synthesized via an Ag^+-induced ion-exchange strategy using BiOI as both a structural and morphological template. The BiOI: $AgNO_3$ mass ratio was found to critically influence the extent of phase transformation and the preservation of the hierarchical architecture. Among the composites, the BA-50:50 sample exhibited the highest photocatalytic activity, maintaining partial flower-like morphology and achieving a pseudo-first-order rate constant 1.6 times and 40 times higher than those of pristine BiOI and AgI, respectively. This enhanced performance is attributed to the construction of an efficient Z-scheme heterojunction, which facilitates directional charge transfer while retaining the strong redox capabilities of both semiconductors. These results demonstrate that morphology-derived advantages from BiOI can be functionally integrated into Bi_2O_3/AgI systems to improve photocatalytic efficiency under visible-light irradiation significantly. Moreover, the mild, room-temperature synthesis route developed in this work offers a scalable and sustainable pathway for designing high-performance photocatalysts for environmental remediation applications.

Acknowledgements

This work was supported by the Department of Physics, Faculty of Science, Silpakorn University.

References

[1] S. Kato, and Y. Kansha, "Comprehensive review of industrial wastewater treatment techniques," *Environmental Science and Pollution Research*, vol. 31, pp. 51064–51067, 2024.

[2] S. Thueanbangyang, K. Singsumphan, V. Atimayulerd, C. Nakmuk, C. Suwanchawalit, and M. Aiempanakit, "Synthesis temperature-driven enhancements in BiOI photocatalysis: A hydrothermal approach, " *Journal of Metals, Materials and Minerals*, vol. 35, no. 3, p. e2318, 2025.

[3] D. Daskalova, G. A. Flores, U. Plachetka, M. Möller, J. Wolters, T. Wintgens, and M. C. Lemme, "Combined structural and plasmonic enhancement of nanometer-thin film photocatalysis for solar-driven wastewater treatment," *ACS Applied Nano Materials*, vol. 6, pp. 15204–15212, 2023.

[4] F. K. Algethami, M. R. Elamina, and B. Y. Abdulkhair, "Simple preparation of a sunshine -like bismuth oxyiodide nanosheets for photocatalytic degradation of organic pollutant under sunlight," *Journal of Optoelectronic and Biomedical Materials*, vol. 1, pp. 57–65, 2021.

[5] L. Huidobro, A. Domingo, E. Gomez, and A. Serra, "Bismuth oxyiodide-based composites for advanced visible-light activation of peroxymonosulfate in pharmaceutical mineralization," *Chemosphere*, vol. 366, p. 143532, 2024.

[6] J.-W. Zhao, Z.-Q. Wei, S.-P. Huang, L. Li, and J.-H. Ma, "Photocatalytic properties of bismuth oxyiodide nanomaterials with different morphologies," *Desalination and Water Treatment*, vol. 281, pp. 287–295, 2023.

[7] M. R. Elamin, K. H. Ibnaouf, N. Y. Elamin, F. A. Adam, A. H. Alolayan, and B. Y. Abdulkhair, "Spontaneous adsorption and efficient photodegradation of indigo carmine under visible light by bismuth oxyiodide nanoparticles fabricated entirely at room temperature," *Inorganics*, vol. 10, no. 5, p. 65, 2022.

[8] J. Luo, X. Zhou, L. Ma, and X. Xu, "Enhanced visible-light-driven photocatalytic activity of WO_3/BiOI heterojunction photocatalysts," *Journal of Molecular Catalysis A: Chemical*, vol. 410, pp. 168–176, 2015.

[9] Y. Guan, J. Wu, Xi. Man, Q. Liu, Y. Qi, P. He, and X. Qi, "Rational fabrication of flower-like BiOI1-x photocatalyst by modulating efficient iodine vacancies for mercury removal and DFT study," *Chemical Engineering Journal*, vol. 396, p. 125234, 202010.

[10] K. Ren, K. Zhang, J. Liu, H. Luo, Y. Huang, and X. Yu, "Controllable synthesis of hollow/flower-like BiOI microspheres and highly efficient adsorption and photocatalytic activity," *Crystal Engineering Communications*, vol. 14, pp. 4384–4390, 2012.

[11] Y. Bu, J .Xu, Y. Li, Q. Liu, and X. Zhang, "Enhanced photocatalytic activity of BiOI under visible light irradiation by the modification of MoS_2," *Royal Society of Chemistry*, vol. 7, pp. 42398–42406, 2017.

[12] J. Jiang, Z. Mu, P. Zhao, H. Wang, and Y. Lin, "Photo-generated charge behavior of BiOI/g-C_3N_4 photocatalyst in photoreduction of Cr(VI): A novel understanding for high-performance," *Materials Chemistry and Physics*, vol. 252, p. 123194, 2020.

[13] T. Zhang, Z.-C. He, Q. Mei, W. Peng, Q.-Z. Wang, H.-F. Cheng, and F. Ding, "Monolayer BiOI doped with nonmetals (B, C, N, Si, P, S) to enhance photocatalytic hydrogen precipitation performance," *Applied Surface Science*, vol. 669, p. 160560, 2024.

[14] H. Wang, Y. Liang, L. Liu, J. Hu, P. Wu, and W. Cui, "Enriched photoelectrocatalytic degradation and photoelectric performance of BiOI photoelectrode by coupling rGO," *Applied Catalysis B: Environmental*, vol. 208, pp. 22–34, 2017.

[15] S. Luo, C. Tang, Z. Huang, C. Liu, J. Chen, and M. Fang, "Effect of different Bi/Ti molar ratios on visible-light photocatalytic activity of BiOI/TiO_2 heterostructured nanofibers," *Ceramics International*, vol. 42, pp. 15780–15786, 2016.

[16] Z. Liu, X. Xu, J. Fang, X. Zhu, J. Chu, and B. Li, "Micro-emulsion synthesis, characterization of bismuth oxyiodine/ titanium dioxide hybrid nanoparticles with outstanding photo-catalytic performance under visible light irradiation," *Applied Surface Science*, vol. 258, pp. 3771– 3778, 2012.

[17] L. Hu, Y. Liao, D. Xia, Q. Zhang, H. He, J. Yang, Y. Huang, H. Liu, F. Zhang, C. He, and D. Shu, "In-situ fabrication of AgI-BiOI nanoflake arrays film photoelectrode for efficient wastewater treatment, electricity production and enhanced recovery of copper in photocatalytic fuel cell," *Catalysis Today*, vol. 339, pp. 379–390, 2020.

[18] J. Lv, Q. Hu, C. Cao, and Y. Zhao, "Modulation of valence band maximum edge and photocatalytic activity of BiOX by incorporation of halides," *Chemosphere*, vol. 191, pp. 427–437, 2018.

[19] J. Cao, Y. Zhao, H. Lin, B. Xu, and S. Chen, "Facile synthesis of novel Ag/AgI/BiOI composites with highly enhanced visible light photocatalytic performances," J*ournal of Solid State Chemistry*, vol. 206, pp. 38–44, 2013.

[20] Q. Wang, X. Shi, E. Liua, J. C. Crittenden, X. Ma, Y. Zhanga, and Y. Cong, "Facile synthesis of AgI/BiOI-Bi_2O_3 multi-hetero-junctions with high visible light activity for Cr(VI) reduction, " *Journal of Hazardous Materials*, vol. 317, pp. 8–16, 2016.

[21] K. A. Reyna-Cavazos, A. Martínez-de la Cruz, D. Contreras, and F. E. Longoria-Rodríguez, "Polyol-assisted coprecipitation synthesis of BiOI photocatalyst and its activity to remove NO_x, " *Research on Chemical Intermediates*, vol. 48, pp. 949–967, 2022.

[22] X. Xie, S. Wang, Y. Zhang, J. Ding, Y. Liu, Q. Yan, S. Lu, B. Li, Y. Liu, and Q. Cai, "Facile construction for new core-shell Z-scheme photocatalyst GO/AgI/Bi_2O_3 with enhanced visible-light photocatalytic activity," *Journal of Colloid and Interface Science*, vol. 581, pp. 148–158, 2021.

[23] Q. Yan, X. Xie, Y. Liu, S. Wang, M. Zhang, Y. Chen, and Y. Si, "Constructing a new Z-scheme multi-heterojunction photo-cataslyts Ag-AgI/ BiOI-Bi_2O_3 with enhanced photocatalytic activity," *Journal of Hazardous Materials*, vol. 371, pp. 304–315, 2019.

[24] V. Atimayulerd, S. Thueanbangyang, C. Nakmuk, K. Singsumphan, K. Aiempanakit, K. Charoenkitamorn, C. Suwanchawalit, and M. Aiempanakit, "Enhanced visible-light photocatalytic activity of BiOI synthesized via simple solvent engineering," *Optik,* vol. 338, p. 172502, 2025.

[25] M. Aiempanakit, P. Sudjai, K. Singsumphan, S. Laksee, and C. Suwanchawalit, "Brazilein modified zinc oxide nanorods with enchanced visible light-responsive photocatalytic efficiency," *Journal of Metals, Materials and Minerals*, vol. 32, no. 2, pp. 70-76, 2022.

[26] K. Singsumphan, C. Suwanchawalit, W. Somsorod, T. Sripathomkul, P. Sawanglap, K. Aiempanakit, and M. Aiempanakit, "Low-voltage electrophoretic deposition of silver nanoparticles on ZnO nanorods thin films for enhanced visible-light photocatalysis," *Optik*, vol. 322, pp. 172179, 2025.

[27] A. Chuenkruit, W. Thongjoon, K. Aiempanakit, M. Aiempanakit, and C. Aiempanakit, "Nanostructure of TiO_2 and WO_3 multilayer films deposited on ITO glass for electrochromic enhanced photocatalytic activity," *Journal of Metals, Materials and Minerals*, vol. 34, no. 4, pp. 1964, 2024.

[28] M. Aiempanakit, J. Sangkaworn, N. Worawannotai, K. Laohhasurayotin, W. Sangchay, S. Lakseee, and C. Suwanchawalit, "Enhancement of visible light-responsive photocatalytic efficiency by using a laccaic acid-modified titanium dioxide photocatalyst," J*ournal of the Brazilian Chemical Society*, vol. 33, no. 6, pp. 541-549, 2022.

[29] D. A. Reddy, J. Choi, S. Lee, R. Ma, and T. K. Kim, "Green synthesis of AgI nanoparticle-functionalized reduced graphene oxide aerogels with enhanced catalytic performance and facile recycling," *Royal Society of Chemistry*, vol. 5, pp. 67394-67404, 2015.

[30] Y. Xu, S. Huang, H. Ji, L. Jing, M. He, H. Xu, Q. Zhan, and H. Li, "Facile synthesis of CNT/AgI with enhanced photo-catalytic degradation and antibacterial ability," *Royal Society of Chemistry*, vol. 6, p. 6905, 2016.

[31] M. Arumugam, K.-K. Seralathan, S. Praserthdam, M. Tahir, and P. Praserthdam, "Synthesis of novel graphene aerogel encapsulated bismuth oxyiodide composite towards effective removal of methyl orange azo-dye under visible light," *Chemosphere*, vol. 303, pp. 135121, 2022.

[32] T. Selvamani, S. Anandan, L. Granone, D. W. Bahnemann, and M. Ashokkumar, "Phase-controlled synthesis of bismuth oxide polymorphs for photocatalytic applications," *Materials Chemistry Frontiers*, vol. 2, no. 9, pp. 1664-1673, 2018.

[33] X. Wang, X. Wan, W. Li, and X. Chen, "One-step hydro-thermal synthesis of the Ag/AgI heterojunction with highly enhancedvisible-light photocatalytic performances," *Micro & Nano Letters*, vol. 9, no. 6, p. 376–381, 2014.

[34] Y. Sun, W.Wang, L. Zhang, and Z. Zhang, "Design and controllable synthesis of a-/γ-Bi_2O_3 homojunction with synergetic effect on photocatalytic activity," *Chemical Engineering Journal*, vol. 211-212, pp. 161-167, 2012.

[35] L. Yosefi, and M. Haghighi, "Fabrication of nanostructured flowerlike p-BiOI/p-NiO Heterostructure and its efficient photo-catalytic performance in water treatment under visible-light irradiation," *Applied Catalysis B: Environmental*, vol. 220, pp. 367-378, 2018.

[36] J. Henle, P. Simon, A. Frenzel, S. Scholz, and S. Kaskel, "Nanosized BiOX (X) Cl, Br, I) Particles synthesized in reverse microemulsions," *Chemistry of Materials*, vol. 19, no. 3, pp. 366-373, 2007.

[37] O. Husberg, H. Vogelsang, and W. von der Osten, "Confined excitons in AgI nanocrystals in crystalline KI matrix," *Journal of Luminescence*, vol. 96, pp. 155–162, 2002.

[38] Q. Yang, J. Huang, J. Zhong, J. Chen, J. Li, and S. Sun, "Charge separation behaviors of novel AgI/BiOI heterostructures with enhanced solar-photocatalytic performance," *Current Applied Physics*, vol. 17, pp. 1202-1207, 2017.

[39] X. Jia, H. Lin, J. Cao, C. Hu, H. Sun, and S. Chen, "Synergistic introduction of oxygen vacancy and silver/silver iodide: Realizing deep structure regulation on bismuth oxybromide for robust carbon dioxide reduction and pollutant oxidation," *Journal of Colloid and Interface Science*, vol. 624, pp. 181-195, 2022.

[40] V. Ruiz-Santoyo, S. García-Carvajal, and M. C. Arenas-Arrocena, "Photocatalytic removal of synthetic dyes using Bi_2O_3–TiO_2 nanocomposites obtained by simple hydrothermal route," *Journal of Nanoparticle Research*, vol. 27, 2025.

[41] S. Madji, M. Belmedani, E. Mekatel, S. Zouaoui, and S. E. I. Lebouachera, "The development of a new $Bi_{12}ZnO_{20}$/AgI heterosystem for the degradation of dye-contaminated water by photocatalysis under solar irradiation: Synthesis, characterization and kinetics," *Processes*, vol. 13, pp. 1342, 2025.

[42] M. Mousavi-Kamazani, M. Ghodrati, and R. Rahmatolahzadeh, "Fabrication of Z-scheme flower-like AgI/Bi_2O_3 heterojunctions with enhanced visible light photocatalytic desulfurization under mild conditions." *Journal of Materials Science: Materials in Electronics*, vol. 31, pp. 5622-5634, 2020.

[43] Z. Chuan, H. Yifen, S. Jingtao, H. Shaohua, M. Minfeng, Z. Liang, L. Kaiwen, and G. Yingying, "Enhanced photocatalytic degradation of indigo carmine dye by biomass carbon supported beta-Bi_2O_3 doping with Ag ions." *Journal of Alloys and Compounds*, vol. 1024, pp. 180163, 2025.

[44] M. Vautier, C. Guillard, and J.-M. Herrmann, "Photocatalytic degradation of dyes in water: Case study of indigo and of indigo carmine." *Journal of Catalysis*, vol. 201, no. 1, pp. 46-59, 2001.